Available online at www.sciencedirect.com
SCIENCE DIRECT®
Journal of Power Sources 124 (2003) 261–265
JOURNAL OF POWER SOURCES
www.elsevier.com/locate/jpowsour

Short communication

Investigation of cycle life of Li–$Li_xV_2O_5$ rechargeable batteries

P.L. Moss [a], R. Fu [b], G. Au [c], E.J. Plichta [c], Y. Xin [d], J.P. Zheng [a,e,*]

[a] *Department of Electrical and Computer Engineering, Florida A&M University and Florida State University, Tallahassee, FL 32310, USA*
[b] *Center for Interdisciplinary Magnetic Resonance, National High Magnetic Field Laboratory, Florida State University, Tallahassee, FL 32310, USA*
[c] *US Army Communications-Electronics Command, Ft. Monmouth, NJ 07703, USA*
[d] *The Magnet Science and Technology, National High Magnetic Field Laboratory, Florida State University, Tallahassee, FL 32310, USA*
[e] *Center for Advanced Power Systems, Florida State University, Tallahassee, FL 32310, USA*

Received 1 May 2003; accepted 22 May 2003

Abstract

Li rechargeable cells made with structural the arrangement Li/membrane/$Li_xV_2O_5$ were examined under different charge states using AC impedance, environmental scanning electron microscope (ESEM) and transmission electron microscope (TEM). These states include charged, discharged, and over-cycled. The lowest internal resistance was obtained from the cell in the charged state; the resistance increased when the cell was discharged; and the highest resistance was obtained from the cell in the over-cycled state. From the ESEM and TEM studies, it was found that the surface of the cathode was porous initially; however, it was coated with an amorphous film and porous features had also disappeared from the cell in the over-cycled state. In addition, higher concentration of aluminum was found on the surface of the cathode in over-cycled cells. The mechanisms for capacity degradation are discussed.

Keywords: Capacity degradation; LiV_2O_5; AC impedance; Surface morphology

1. Introduction

A Li rechargeable battery is formed from three active components that include a metallic lithium (Li) anode, a lithium-ion-conducting electrolyte, and a lithium insertion cathode (such as $Li_xM_yO_z$, M: V, Mn, Co, Ni) [1–3]. During cell discharge and charge, Li is inserted into and extracted from the host structures of the cathode electrodes, respectively. The ideal electrode material and electrolyte for Li rechargeable batteries should have outstanding electrochemical performance and a stable capacity upon extended cycling. However, degradation of the anode, cathode and electrolyte always occur during the cycling. Various mechanisms that caused the capacity degradation and decreased cycle life of a battery are reported by different groups. For example, the decomposition of organic electrolytes with gas generation during charge and discharge cycling has been found [4–7]. This process results in depletion of the solvent in the electrolyte and deposition of Li [8] and other films [7] on the electrode surfaces. The depletion of the solvent and deposition of thin films developed in the batteries contribute toward the increase in battery impedance and shortend battery life. It was also found that the charge and discharge cycling of cathodes caused microstructural damage and cation disorder [9,10]. It was believed that breakdown of the oxide cathode material due to repeated lattice contraction and expansion appears to be an important failure mode in the oxide electrodes [10]. It was also reported that dendritic electrodeposition of Li had been obtained in Li–polymer cells [11,12]. Li dendritic growth will eventually short the battery. In this paper, we report recent results on cycling Li–$Li_xV_2O_5$ button cells using AC impedance and microscopic analysis techniques. The results combined with our previous studies using nuclear magnetic resonance (NMR) provide a clear understanding of the cycle life of these cells.

2. Experimental

Panasonic® vanadium pentoxide (V_2O_5) Li-rechargeable batteries were used as the experimental samples. The button cell batteries comprised Li (anode)/membrane/$Li_xV_2O_5$ (cathode), and were rated at 30 mAh. The aluminum (Al) mesh and stainless steel bottom case of the button cell were used as the current collectors for the anode and cathode, respectively. The cells are 23 mm in diameter and 2.0 mm in thickness.

* Corresponding author. Tel.: +1-850-410-6464; fax: +1-850-410-6479.
E-mail address: zheng@eng.fsu.edu (J.P. Zheng).

0378-7753/$ – see front matter © 2003 Elsevier B.V. All rights reserved.
doi:10.1016/S0378-7753(03)00734-1

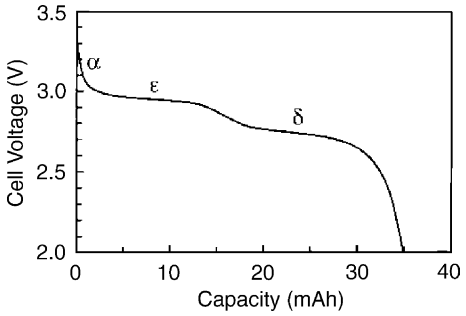

Fig. 1. Voltage–capacity curve of Li/membrane/$Li_xV_2O_5$ cell during discharge process.

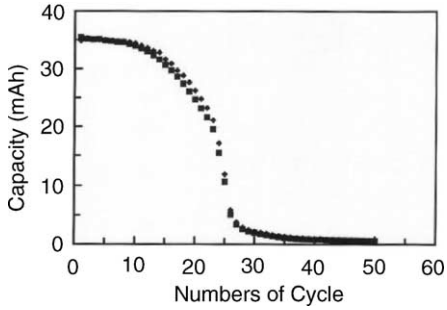

Fig. 2. Capacities of the cell as a function of cycle numbers during discharge process at 25 °C. Symbols of (◆) and (■) represent charge and discharge capacities.

An Arbin battery test system was used for charge and discharge cycling of the cells. During the charge cycle, a constant voltage mode of 3.4 V was used and during discharge, a constant current of 10 mA was used. A Solartron electrochemical measurement unit (model 1280B) was used to measure the AC impedance spectra in a frequency range from 0.01 Hz to 20 kHz at room temperature. During AC impedance measurements, a sinusoidal source with an amplitude of 10 mV was applied to the cell. An integral step of 2 s was also used to increase the accuracy at each frequency point to offset the error due to the presence of noise in the lines connecting the spectrometer to the battery.

Three different samples for microscopic studies were prepared as follows: One charged cell was charged to 3.4 V at constant voltage; one discharged cell was discharged to 2.1 V at 10 mA; and one over-cycled cell was continuously charged and discharged until the cell had capacity close to zero. These cells were then opened, and the $Li_xV_2O_5$ cathode electrode materials were removed from cells in a glove box filled with argon gas.

An environmental scanning electron microscope (ESEM) was used for imaging the surface morphology of the electrodes. The energy dispersive X-ray spectroscope (EDX) built into the ESEM system was employed to analyze the chemical composition of the electrode. A Jeol-2010 transmission electron microscope (TEM) operated at 200 kV with selected area electron diffraction (SAED) built into the TEM system were used to investigate the microstructures of the cathode materials including particle morphology and crystalline structures.

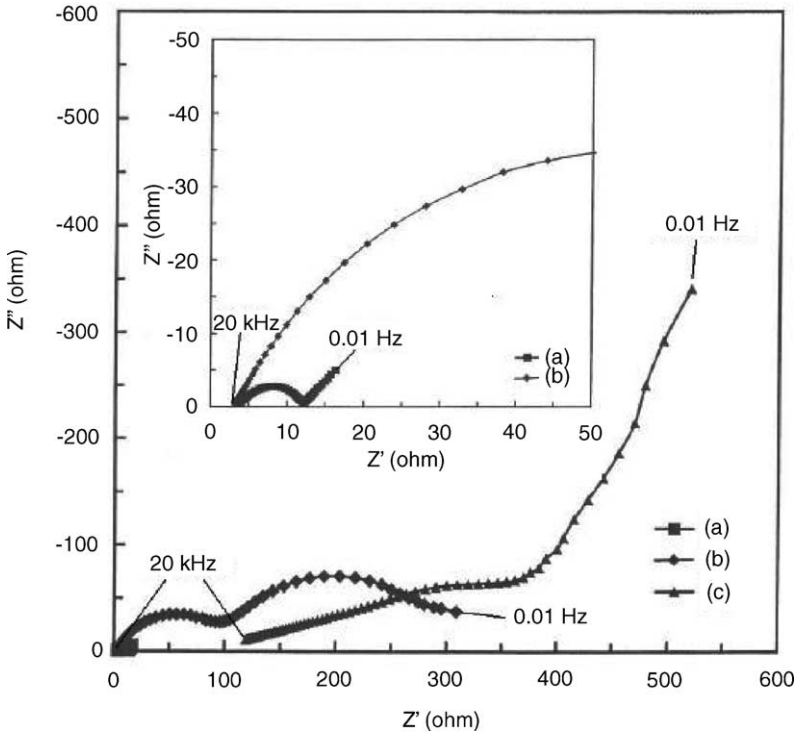

Fig. 3. Nyquist plots of cells in the (a) charged, (b) discharged, and (c) over-cycled states in the frequency range from 0.01 Hz to 20 kHz at room temperature.

3. Results and discussion

Fig. 1 shows the voltage–capacity curve during discharge at 25 °C. Plateaus are observed from 3.4 to 2.0 V and comparing these plateaus to previous work [15–17], it has been determined that in this voltage discharge interval the $Li_xV_2O_5$ structure undergoes at least three distinct phase changes, α, ε, and δ each with a different *x*-value of Li insertion. When the cell was charged to 3.4 V, the $Li_xV_2O_5$ was α-phase with a Li concentration of $0.1 < x < 0.2$; when the cell was discharged to 2.1 V, it was δ-phase with a Li concentration of $1.6 < x < 1.8$.

Fig. 2 shows the charge and discharge capacities as a function of number of cycle at about 25 °C. The battery was cycled from 2.1 to 3.4 V. It can be seen that the initial capacity of the cell was about 35 mAh; however, after 26 cycles, the capacity reduced to less than 15% of the initial capacity. It can also be seen that the discharge capacities at 25 °C as a function of the numbers of cycle were almost identical to the charge capacities. It was found that the cycle life was insensitive to the minimum discharge voltage in a range from 1.7 to 2.3 V.

Fig. 3 shows Nyquist plot of three cells at 25 °C. The Nyquist plot for the charged cell shows a small semi circle in the frequency range from 0.794 Hz to 20 kHz and a linear plot at an angle of 52° in the frequency range from 0.01 to 0.794 Hz. The semi circle in this plot represents the charge transfer at the electrolyte/electrode interface and the linear portion of this plot (0.01 to ∼0.794 Hz) represents the diffusion of Li into the $Li_xV_2O_5$ structure or the phase boundaries in the structure. Upon closer examination it can be seen at a high frequency of 20 kHz there was an electrolyte resistance of about 3.1 Ω. The charge transfer resistance at the electrolyte electrode interface can be determined by Z′ at 0.794 Hz, and was approximately 35–3.1 = 31.9 Ω. The low frequency point (∼0.01 Hz) represents the diffusion of Li in and out of the $L_xV_2O_5$ structure. The Nyquist plot for a discharged cell shows an electrolyte resistance of the same value as that of the charged cell. However, the charge transfer resistance for the discharged cell was greater than 100 Ω. The impedance at low frequency (0.01 Hz) was also much greater than that for the charged cell. The increase in charge transfer resistance and impedance at low frequency can be understood by the fact that the concentrations of Li ions in the electrode surface region and in $Li_xV_2O_5$ were high, and as a result the diffusion of Li ions in and out of the surface region and the structure were low. The Nyquist plot from the over-cycled cell shows a dramatic increase in the electrolyte resistance at 20 kHz which is directly related to a decrease in ionic conductivity. This decrease in conductive indicates a decrease in cycle life. At both high and low frequencies the transport of Li ions flowing from the anode to the $Li_xV_2O_5$ structure was very low.

After the AC impedance spectral measurements, active materials inside the button cell were removed from the case. Two noticeable differences from the cathode electrode in charged (or discharged) and over-cycled cells were visible. The first is that the cathode electrode from the over-cycled cell was dryer than that from the charged or discharged cells. Secondly, the color of the cathode was black for the electrode from the charged and discharged cells, but became dark-yellow for the electrode from the over-cycled cell. The color on the Li anode electrodes at different charge states was also different. The anode electrode in the discharged state was dark-silver, which is the natural color of Li foil; however, the anode in the charged and over-cycled states were black, which was believed to be due to a layer of Li film with high porosity [14].

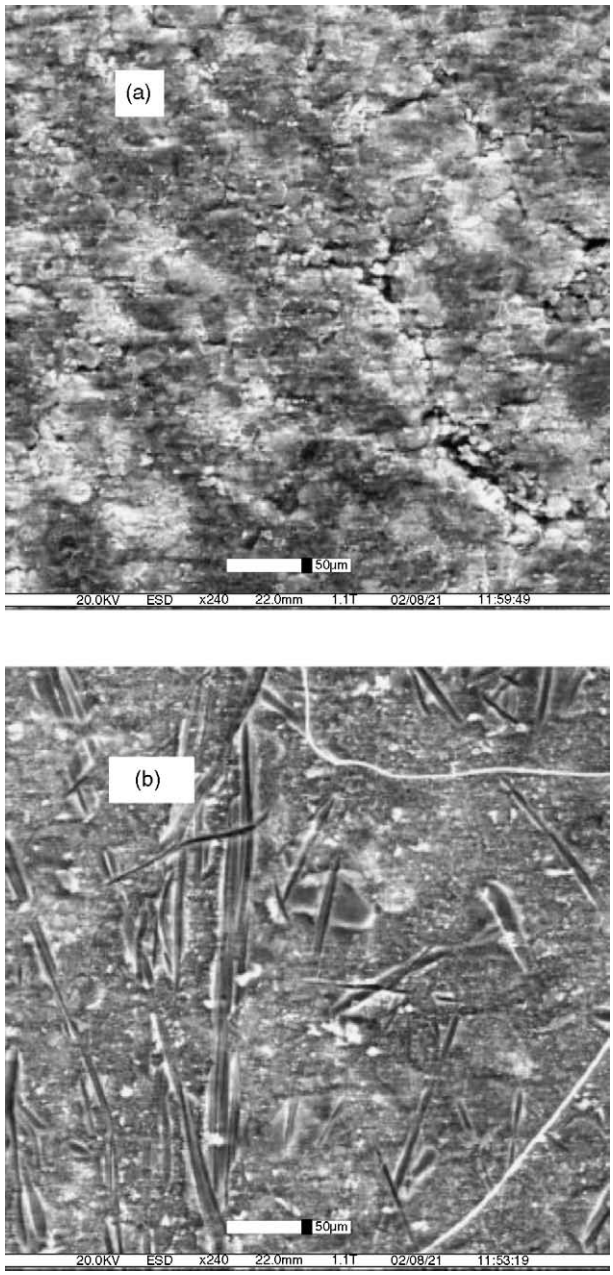

Fig. 4. ESEM images of cathode surfaces from (a) charged and (b) over-cycled cells. The surface faced the membrane in the cell.

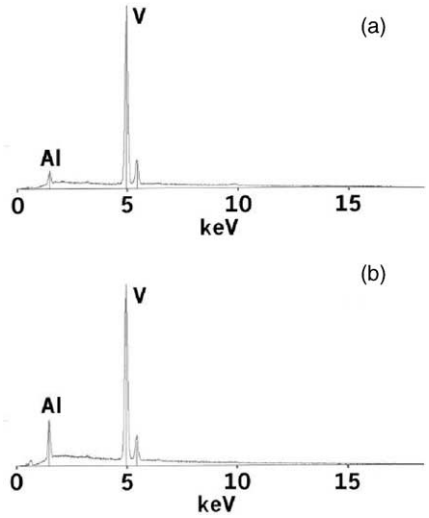

Fig. 5. EDX spectra measured from surfaces of cathode electrodes from (a) charged and (b) over-cycled cells.

In order to closely examine the cathodes in electrodes discharged states, the ESEM system was used to study the surface morphology and chemical composition. Fig. 4(a) and (b) shows surface morphologies of the $Li_xV_2O_5$ cathode at the interface with the membrane for cells from charged and over-cycled states, respectively. It can be seen from Fig. 4(a) that the electrode had microsize particles; the boundary between the particles could clearly be seen. Voids and grooves up to 10 μm could also be observed. Similar surface morphology was obtained from the cathode of the discharged cell. However, from Fig. 4(b) for an over-cycled cell, the boundaries between particles could not be identified. The voids and grooves had also disappeared. The lines on the surface are traces of the membrane surface.

The chemical compositions at the cathode surface were analyzed using EDX. The system can only detect elements that are heavier than oxygen; therefore, Li and other components from the electrolyte could not be identified. Fig. 5(a) and (b) shows EDX spectra of cathode electrode surfaces from the charged and over-cycled cells, respectively. From

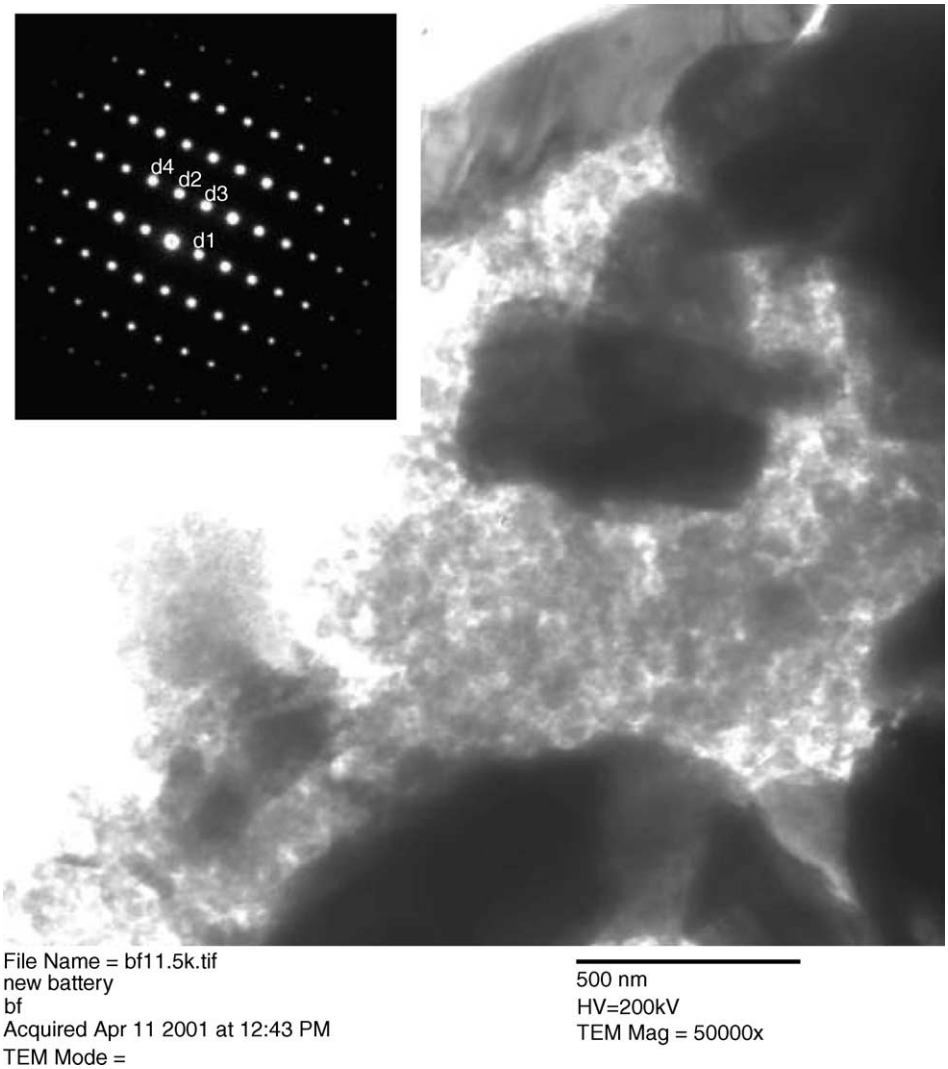

Fig. 6. TEM image of cathode material from a charged cell. The insert is the SAED pattern from the large particle.

both electrodes, besides the V element, an unexpected Al element was detected at 1.487 keV. However, the intensity of the Al signals from the over-cycled cell was higher than that from charged cell. The result indicated that the Al was deposited on the surface of cathode during the charge and discharge cycle; the only source for Al in the cell is the current collector from the Li anode electrode. The Al must have been dissolved in the electrolyte before the deposition on the cathode. The Al distribution inside the cathode was also investigated by mapping the Al signal on a cross-section of cathode. It was found that in general the Al concentration inside the electrode was much lower than that on the surface of electrode, and was quite nonuniformly distributed inside the electrode. This observation is reasonable, since the deposition would occur on the surface and along the boundaries of particles. Therefore, where the voids and grooves existed, it would have a high concentration of Al.

TEM was also used to image particles on the cathode. Fig. 6 shows a TEM image of the cathode material from a charged cell. From TEM images, we can see that two different groups of materials were found in the electrode. The majority of the material was formed with large particles of the order of μm. The SAED patterns indicated that the large particles were single crystalline phase $Li_xV_2O_5$, close to the crystal structure of V_2O_5. Amorphous regions containing small particles were also present, these amorphous regions have a high amount of Al from EDX analysis. From both TEM and EDX results, there is no ascertainable difference in the general features three cells at different charge states including the over-cycled state. It indicates that no microstructural damage occurred in V_2O_5 crystals.

The microscopic studies including ESEM and TEM are consistent with our NMR studies [13]. There were almost identical ^{51}V NMR spectra obtained from charged and over-cycled $Li_xV_2O_5$ samples, which suggested that the capacity degradation and cycle life of Li–$Li_xV_2O_5$ cells was not due to the degradation such as structural damage or cation disorder in the cathode [13]. Also, from the high-resolution ^{7}Li NMR spectra, two groups of Li were obtained from the cathode of charged and discharged cells, they were located inside and outside of the V_2O_5 structure; however, only the Li located outside of V_2O_5 structure was obtained from the cathode of an over-cycled cell. After considering all experimental observations, we suggest that the capacity degradation and cycle life of Li–$Li_xV_2O_5$ cells are due to the decomposition of organic electrolyte during charge and discharge. This process would result in depletion of the solvents in the electrolyte and also deposition of Li, Al, and other materials on the surface of the cathode, which reduced the porosity of the electrode. The depletion of the solvent and deposition of a thin film on the cathode caused the increase of cell impedance and reduction of battery life. The degradation mechanism for these Li–$Li_xV_2O_5$ cells is similar to Li–MoS_2 cells [6].

4. Conclusion

From AC impedance spectra of charged, discharged, and over-cycled Li–$Li_xV_2O_5$ cells, it was found that the ionic conductivity of the electrolyte and Li diffusivity into the electrodes were significantly low in an over-cycled cell. From microscopic studies, it was found that the porosity of the cathode electrode was reduced due to amorphous film deposition during charge and discharge. It is believed that the capacity degradation of the cell is mainly due to the decomposition of the organic electrolyte during charge and discharge. The decomposition process resulted in depletion of the solvent in the electrolyte and deposition of Li, Al, and other materials on the surface of V_2O_5 particles.

Acknowledgements

This work was partially supported by US Army Communications-Electronics Command. YX thanks NHMFL funded by NSF under cooperative agreement DMR-0084173 and the State of Florida.

References

[1] P. Baudry, S. Lascaud, H. Majastre, D. Bloch, J. Power Sources 68 (1997) 432–435.
[2] K. Murata, S. Izuchi, Y. Yoshihisa, Electrochim. Acta 45 (2000) 1501–1508.
[3] D. Fauteux, A. Massucco, M. McLin, M. van Buren, J. Shi, Electrochim. Acta 40 (1995) 2185–2190.
[4] Z.X. Shu, R.S. McMillan, J.J. Murray, J. Electrochem. Soc. 140 (1993) 922–927.
[5] E. Cattaneo, J. Ruch, J. Power Sources 43–44 (1993) 341–347.
[6] K. Kumai, T. Ikeya, K. Ishihara, T. Iwahori, N. Imanishi, Y. Takeda, O. Yamamoto, J. Power Sources 70 (1998) 235–239.
[7] H. Yoshida, T. Fukunaga, T. Hazama, M. Terasaki, M. Mizutani, M. Yamachi, J. Power Sources 68 (1997) 311–315.
[8] D. Aurbach, E. Zinigrard, H. Teller, P. Dan, J. Electrochem. Soc. 147 (2000) 1274–1279.
[9] H. Wang, Y.I. Jang, B. Huang, D. Sadoway, Y.M. Chiang, J. Power Sources 81–82 (1999) 594–598.
[10] J.H. Lee, J.K. Hong, D.H. Jang, Y.K. Sun, S.M. Oh, J. Power Sources 89 (2000) 7–14.
[11] C. Brissot, M. Rosso, J.N. Chazalviel, S. Lascaud, J. Power Sources 81–82 (1999) 925–929.
[12] C.W. Kwon, S.E. Cheon, J.M. Song, H.T. Kim, K.B. Kim, C.B. Shin, S.W. Kim, J. Power Sources 93 (2001) 145–150.
[13] Z. Ma, P. Moss, R. Fu, G. Au, E.J. Plichta, J.P. Zheng, J. New Mater. Electrochem. Sys., in press.
[14] J.P. Zheng, P.T. Charbel, H.S. Kwok, Electrochem. Solid-State Lett. 3 (2000) 338.
[15] B. Pecquenard, D. Gonvier, N. Baffier, Solid-State Ionics 78 (1995) 287.
[16] J.M. Cocciantelli, M. Menetrier, C. Delmas, J.P. Doumerc, M. Pouchard, P. Hagenmuller, Sloid-State Ionics 50 (1992) 99.
[17] J.M. Cocciantelli, J.P. Doumerc, M. Pouchard, M. Broussely, J. Labat, J. Power Sources 34 (1991) 103.